08,13

Effect of continuous-wave CO_2 Laser beam scan rate on the composition of laser-induced graphene

© R.G. Zonov, V.L. Vorobyov, F.Z. Gil'mutdinov, T.N. Mogileva, G.M. Mikheev

Udmurt Federal Research Center, Ural Branch Russian Academy of Sciences,
Izhevsk, Russia

E-mail: mikheev@udman.ru

Received July 11, 2025
Revised August 6, 2025
Accepted August 13, 2025

Film samples of laser-induced graphene (LIG) were synthesized on the surface of polyimide film through line-by-line scanning with a focused beam of a continuous-wave carbon dioxide laser. The structure and chemical composition of the near-surface layer of the synthesized material were investigated as a function of the scanning speed v of the laser beam. It was found that a decrease in v from 400 to 10 mm/s leads to an increase in nitrogen concentration by more than 11 times. At an optimal laser power of 0.55 W and a speed of $v = 10$ mm/s, the nitrogen concentration reaches 5.7 at.%. It has been demonstrated that the increase in nitrogen concentration with a decrease in v occurs due to the pyridine and pyrrole configurations of nitrogen in the nanocrystalline structure of graphite, which is accompanied by a significant reduction in the sheet resistance of LIG. The obtained results correlate with the previously established multiple increase in the electrochemical capacitance of LIG with a decrease in v.

Keywords: polyimide film, laser pyrolysis, X-ray photoelectron spectroscopy, elemental composition, nitrogen doping.

DOI: 10.61011/PSS.2025.08.62275.184-25

1. Introduction

The first quarter of the twenty first century was marked by explosive development of nanotechnologies, which resulted in discovery of graphene and other nanocarbon materials that have great potential for practical applications. One of these materials is laser-induced graphene (LIG), which was synthesized for the first time on a polyimide film by a method of laser pyrolysis of its subsurface layer in air under normal conditions using a pulse carbon-dioxide laser [1]. The LIG is a high-porosity conducting film structure, which consists of nanocrystallites of turbostratic graphite, whose Raman light scattering spectrum resembles a Raman spectrum of graphene with defects [2]. Thanks to technological simplicity of synthesis, the LIG film structures are of high interest for various applications and widely used when designing and creating diverse electronic devices of various purpose, varied gauges and sensors. They include sensors for various gases [3–5], photodetectors [6–8], various flexible human body-portable biosensors [9,10], microsupercapacitors [11–15], etc.

Various carbon-containing materials can be used as a precursor for LIG synthesis [16–20]. It is known that the LIG can be produced on a surface of organic materials, for example, on wood, bread and on a coconut surface [21]. However, a widespread precursor for LIG synthesis is a polyimide film [22–24], which is commercially produced. It has excellent elasticity and thermal stability, thereby making it possible to produce flexible LIG film structure on its surface for creating various electronic devices.

The LIG on the polyimide film can be synthesized using pulse [1,4] or continuous-wave CO_2-lasers [6,13,25] with the wavelength of 10.6 μm as well as by applying short-wave diode lasers with the wavelength 405 and 450 nm [10,26,27], whose radiation is well absorbed by the polyimide film [28]. Other lasers are also used for LIG synthesis on the surface of the polyimide film, for example, femtosecond lasers designed to operate at other wavelengths [29].

The LIG synthesized on the surface of the polyimide film can be used as electrodes for producing flexible microsupercapacitors. These LIG electrodes can be produced by well-suited continuous-wave CO_2-lasers that have power of up to several tens of watts and are commercially available for cutting wood and plastics. With the power at a level of just several watts, they allow synthesizing LIG with much higher capacity than in case of application of the pulsed diode lasers.

It is known that electric capacitance of the LIG electrodes that are synthesized in line-by-line scanning of a laser beam along the surface of the polyimide film significantly depends on their thickness, specific surface area and electrical properties. These LIG parameters are in turn affected by synthesis modes, such as a laser power P, a diameter of the focused beam d, a speed of beam motion v in line-by-line scanning and a distance between the lines [13,30,31]. Electric capacitance of the LIG can be also increased by doping a carbon frame with heteroatoms, such as N, B, S and P [32,33]. Of the listed elements, the N atoms are contained in a composition of the very polyimide film (an initial precursor for LIG synthesis), which consists of imidic

and aromatic groups (see, for example, the study [34]). During laser pyrolysis of the polyimide film covalent bonds C−N, C−O and C=O are broken; as a result low-molecular gases are released and an atomic structure of the subsurface layer of the film is changed and rebuilt to form a graphene-like material. At the same time, nitrogen atoms can be embedded in a crystal structure of the carbon material, which was observed in many studies for LIG synthesis on the surface of the polyimide film [32,35–37]. The LIG formation process and the LIG elementary composition, in particular, the N concentration, can be affected by the laser synthesis modes. However, except for some papers [16,37], which investigated the influence of laser power on the LIG elementary composition, such studies do not exist.

We have recently shown that electric capacitance of the LIG electrodes that are synthesized on the surface of the polyimide film can be increased by many times by decreasing a continuous-wave CO_2-laser beam scanning speed and tuning the laser power [38]. The detected effect was explained by an increase of the thickness and the specific surface area of the synthesized nanocarbon material. However, another essential factor that results in the increase of electric capacitance of the LIG can be variation of the concentration of the nitrogen atoms in the synthesized material. In this regard, it is interesting to investigate the influence of the laser beam scanning speed on the elemental and chemical composition of the LIG during its synthesis, which is an aim of the present study.

2. Objects and methods of research

The LIG film structure was formed on the surface of the Kapton H polyimide film wit the thickness of $h = 200\,\mu$m, which was purchased from LLC „Estrokom", Moscow (TU 6-19-102-78 with amend. 1−3, batch № P1826C). The film is a semitransparent material that has a characteristic saturated red-brown color. The spectral dependences of optical constants of the studied film, which are found in the wavelength range 240−2500 nm, are given in the study [28]. The LIG was synthesized by means of the continuous-wave CO_2-laser ($10.6\,\mu$m) in air by line-by-line scanning of the focused beam with the diameter of $120\,\mu$m. The line-by-line motion of the laser beam along the surface of the polyimide film was carried out by means of two reflecting mirrors installed on an automated two-axis table. The laser power in relative units (as a percentage of the maximum power) P_{per}, the speed v of beam motion along the line and the distance between the lines ($25\,\mu$m) were programmatically pre-defined in a laser operation control unit. The actual laser radiation power P incident to the polyimide film was determined by a pre-measured calibration dependence $P(P_{\text{per}})$. The laser beam motion speed v varied within the range from 10 to 400 mm/s. Top speed of 400 mm/s was limited by parameters of the laser beam scanning system, and for $v < 10$ mm/s it was difficult to obtain the good-quality LIG films due to strong warping of the polyimide film. In the experiments, the LIG samples of the size of 10×10 mm were synthesized at various P and v. At the same time, for each fixed speed v the power $P = P_{\text{opt}}$ was selected, at which electric capacitance of the LIG film structure synthesized at this speed v was the highest [38]. As a result, for studies, at quasi-permanent laboratory conditions (during one working day) seven pairs of the LIG samples were manufactured in air and their designations and synthesis modes are listed in the table.

Modes of synthesis of the studied LIG samples

Designation of the samples	Synthesis conditions	
	Speed v, mm/s	Power P_{opt}, W
v_10_P_0.55	10	0.55
v_20_P_0.69	20	0.69
v_30_P_0.8	30	0.8
v_60_P_1.2	60	1.2
v_120_P_2.0	120	2
v_220_P_3.1	220	3.1
v_400_P_4.5	400	4.5

The chemical composition of the LIG subsurface layer was studied by X-ray photoelectron spectroscopy (XPS) in an updated spectrometer ES-2401. Photoelectrons were excited using X-ray radiation MgK_α with a quantum energy of 1253.6 eV. The energy scale of the spectrometer is calibrated by electron binding energies of Au $4f_{7/2}$ (84.0 eV) and Cu $2p_{3/2}$ (932.8 eV). The value of full width at half maximum (the FWHM parameter) of the peak of Au $4f_{7/2}$ is 1.0 eV. The obtained XPS spectra were processed using the CasaXPS software package (version 2.1.34). At the same time, the concentration of the elements was determined with a relative error of ±3 %. During the XPS studies, a sample of highly-oriented pyrolytic graphite (HOPG) was used as a reference. In order to carry out the XPS studies, the LIG film structures were synthesized on the polyimide film fixed on a glass substrate by a double-sided carbon adhesive tape.

The synthesized LIG samples were also studied using an Raman spectrometer (HORIBA HR800). The Raman spectra were excited by radiation of a He-Ne laser at the wavelength of $\lambda_{\text{ex}} = 632.8$ nm. A ×50 magnification lens was used when doing so. The resultant spectrum was found by averaging spectra that were recorded in at least five various points of the LIG surface. A scanning-electron microscope (SEM) (Thermo Fisher Scientific Quattro S) was used to obtain a magnified image of the LIG surface. Sheet resistance of the films was measured by a four-point method (JG ST2258C) with measurement electrodes arranged along one line. The sheet resistance was measured with orientation of the electrode line perpendicular and parallel to a direction of laser beam scanning along the surface of the polyimide film.

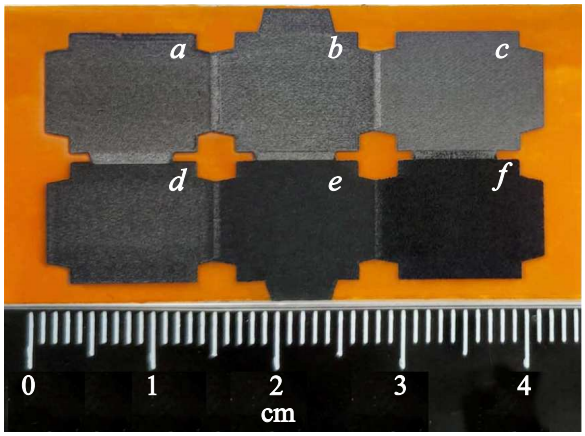

Figure 1. Photos of the six LIG samples synthesized on one piece of the polyimide film at the scanning speeds *a* — 10, *b* — 30, *c* — 60, *d* — 120, *e* — 220 and *f* — 400 mm/s at the optimal powers 0.55, 0.8, 1.2, 2, 3.1 and 4.5 W, respectively.

3. Results and discussion

Figure 1 shows the photos of the six LIG samples produced at the various combined parameters (v, P_{opt}) of laser synthesis on one piece of the polyimide film. It is clear that a color palette of the samples depends on the synthesis modes. The most saturated black color belongs to the sample v_400_P_4.5 that is synthesized at the highest laser beam scanning speed $v = 400$ mm/s. The SEM images of the same LIG samples are shown in Figure 2. It follows from this that the LIG is a spongy material and it consists of interwoven nets of open cavities that are different in shape and size. The LIG surface also exhibits lamellar formations of various spatial orientation. This structure is typical for the LIG synthesized on the surface of the polyimide film and was observed in many studies (see, for example, the studies [6,39,40]). The LIG structure obtained at the high speeds v (Figure 2,*f*) is distinguished by presence of a net of carbon fibers. Such fibers were previously produced on the surface of the polyimide film during its pyrolysis by pulse [41] and continuous [30,42] radiation of the CO_2-laser.

The typical Raman spectrum of the nanocarbon film structure synthesized when $v = 30-400$ mm/s is shown in Figure 3, *a*. It includes the well-known D-, G-, D′- and 2D-bands of scattering with the frequency shifts 1330, 1583, 1616 and 2653 cm^{-1}, respectively. This Raman spectrum is typical for the LIG and is described in a large number of the studies (see, for example, the studies [17,23,38,43]). The scattering spectrum has also a band D+D′ with the frequency shift of 2923 cm^{-1}, which is a combination of the D- and D′-bands [44,45]. Generally, this Raman spectrum is also typical for the carbon nanofibers [46]. It is known that the Raman spectra of defective graphene and graphite contain all the listed scattering bands. But their spectra significantly differ from the spectrum of Figure 3, *a* by the following characteristics of the 2D-band: 1) the spectral form of the band; 2) the value of $\Delta\omega_{2D}$ of the half-width at the half-height; 3) the frequency shift ω_{2D}. The 2D-band of single-layer graphene is described by one Lorentz curve with $\Delta\omega_{2D} = 25\ cm^{-1}$, and the 2D-band of graphite is described by two Lorentz curves that noticeably differ by the frequency shifts. The increase of the number of the graphene layers results in deviation from the Lorentz envelope of the 2D-band with simultaneous increase of its frequency shift ω_{2D} from 2640 cm^{-1} to 2688 cm^{-1} when $\lambda_{ex} = 632.8$ nm [47]. It follows from Figure 3 that the 2D-band of our synthesized material with $\omega_{2D} \approx 2653\ cm^{-1}$

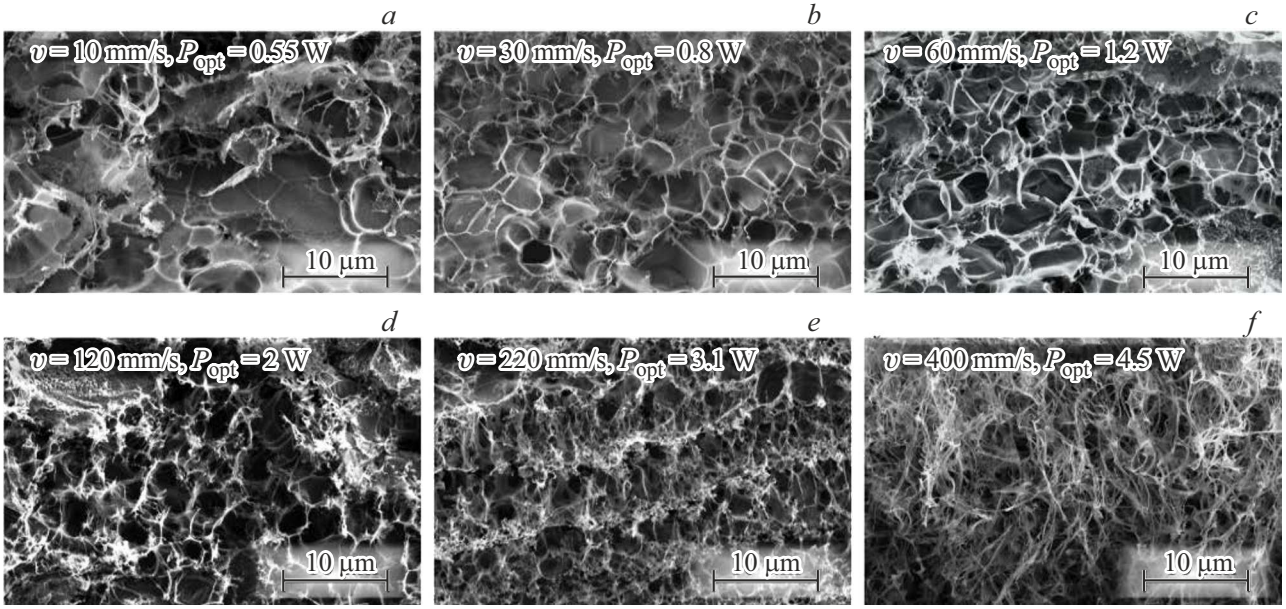

Figure 2. SEM images of the six LIG samples synthesized at the scanning speeds *a* — 10, *b* — 30, *c* — 60, *d* — 120, *e* — 220 and *f* — 400 mm/s at the optimal powers 0.55, 0.8, 1.2, 2, 3.1 and 4.5 W, respectively.

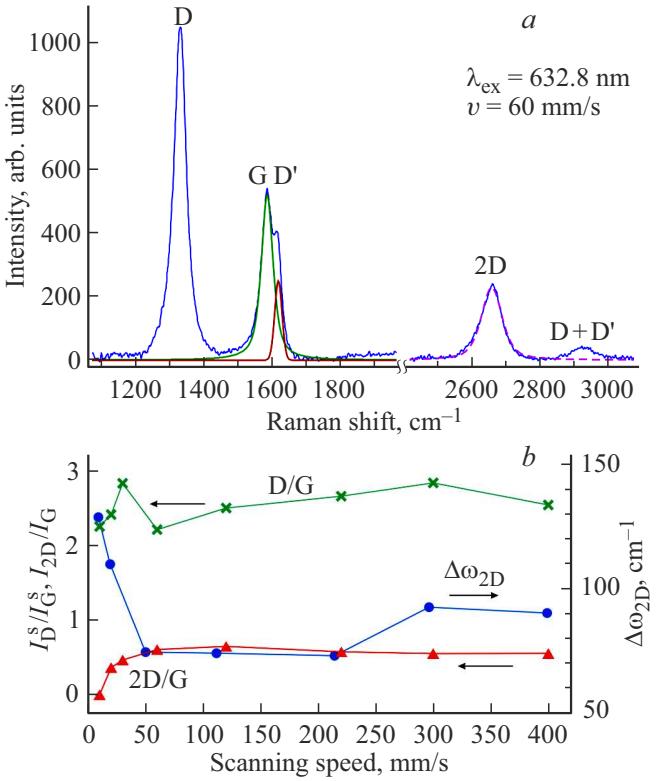

Figure 3. *a* — the Raman spectrum of the LIG synthesized at $v = 60$ mm/s, $P_{opt} = 1.2$ W (the dashed line marks approximation of a 2D-band by the Lorentz function); *b* — the dependences of the ratios I_D^s/I_G^s, I_{2D}/I_G and $\Delta\omega_{2D}$ which characterize the Raman spectra, on the laser beam scanning speed.

is described by one Lorentz curve. At the same time, depending on the scanning speed $\Delta\omega_{2D}$ takes the values from 73 to 120 cm^{-1}. Whence, it follows that the spectral characteristics of the LIG 2D-band significantly differ from those for graphene and graphite. On the other hand, it is known from literature data that the 2D-band of turbostratic graphite with $\omega_{2D} = 2663$ cm^{-1} (when $\lambda_{ex} = 632.8$ nm) [48] is described by one Lorentz curve with $\Delta\omega_{2D} \approx (50-60)$ cm^{-1} [47,49]. Based on this and data obtained in other studies for high-resolution microscopy (see, for example, the study [1]), it can be assumed that during laser pyrolysis of the polyimide film the carbon material that consists of the turbostratic graphite nanocrystallites is synthesized.

The important parameters of the Raman spectra are integral characteristics I_G^s and I_D^s, which are areas under curves of dependences of intensity of the bands G and D, respectively, on the frequency shift. According to the study [50], the integral characteristics I_G^s and I_D^s can be used to evaluate nanocrystallite sizes L_a along the graphene layers by the formula L_a [nm] $= (2.4 \cdot 10^{-10})\lambda_{ex}^4 (I_D^s/I_G^s)^{-1}$. It follows from Figure 3, *b* that within the wide range of variation of v the ratio I_D^s/I_G^s does not significantly change and takes the minimum and maximum values 2.2 and 2.8 at $v = 60$ and 30 mm/s, respectively. Whence, it follows that when the speed v varies from 10 to 400 mm/s, L_a varies within a small range 13–17 nm. However, it follows from Figure 3, *b* that the ratio I_{2D}/I_G (where I_{2D} and I_G are intensities of the peaks I_{2D} and I_G, respectively) remains virtually unchanged for $v \geq 60$ mm/s, but significantly decreases when $v < 60$ mm/s and vanishes at $v = 10$ mm/s. According to the study [51], disappearance of the 2D-band in the Raman spectrum indicates a significant increase of the concentration of defects in the graphite nanocrystallites. At the same time, according to the Figures 1 and 2, the LIG synthesized at $v = 10$ mm/s differs little in terms of a morphology of its surface from the LIG synthesized, for example, at $v = 30$ mm/s, while its electric capacitance in several times exceeds electric capacity of the LIG synthesized at $v = 30$ mm/s [38].

Figure 4 shows the XPS panoramic spectra for the five LIG samples synthesized at the various modes. It is clear that except for the carbon lines C1s all the spectra exhibit the oxygen lines O1s. The spectra of the samples *v*_10_*P*_0.55 and *v*_30_*P*_0.8 synthesized at the speeds $v = 10$ and 30 mm/s also clearly exhibit the nitrogen lines N1s, but these lines practically do not manifest themselves for the samples *v*_120_*P*_2 and *v*_220_*P*_3.1 synthesized when $v = 120$ and 220 mm/s, respectively.

Figure 5 shows the XPS C1s-spectra for the HOPG reference sample and the three LIG samples synthesized when $v = 10, 60$ and 120 mm/s. The figures 6 and 7 show the spectra of oxygen O1s and nitrogen N1s for the four LIG samples synthesized when $v = 10, 30, 60$ and 120 mm/s.

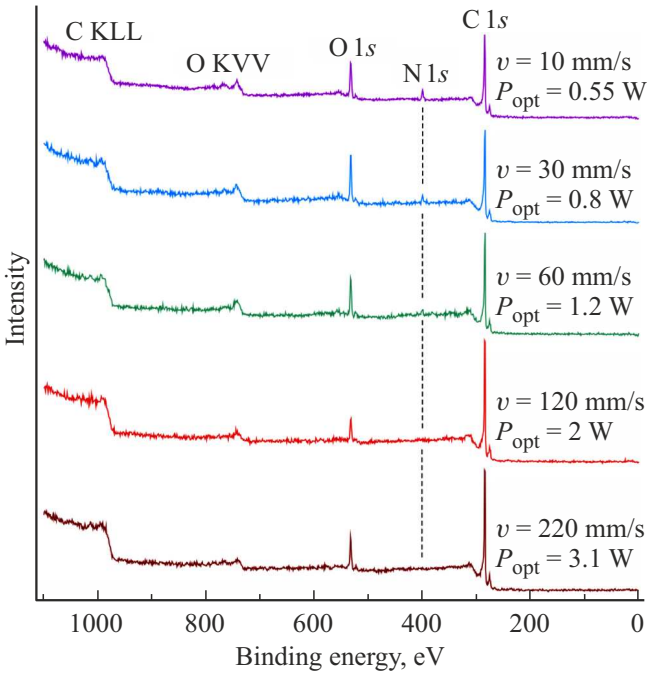

Figure 4. Panoramic XPS spectra of the five LIG samples synthesized at various v and P_{opt}.

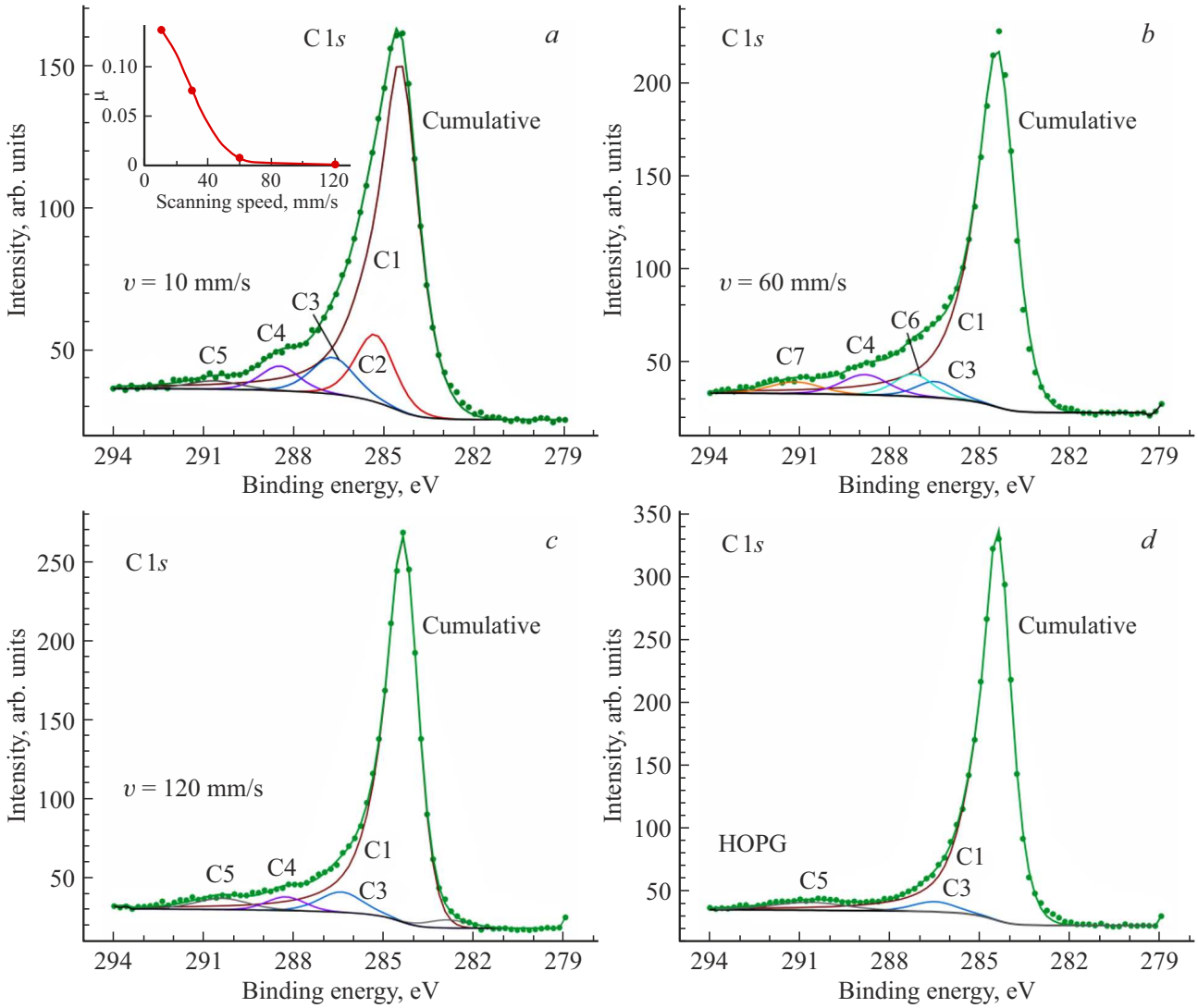

Figure 5. C1s-spectra: of the three LIG samples synthesized at $\upsilon = 10$ (a), 60 (b), 120 mm/s (c) and d — of highly-oriented pyrolytic graphite with the following peaks of binding energy decomposition (by chemical bonds): C1 — 284.4 eV (C−C), C2 — 285.3 eV (C−N), C3 — 286.7 eV (C−O), C4 — 288.5 eV (C=O), C5 — 290.8 eV ($\pi-\pi^*$), C6 — 287.2 eV, C7 — 291.2 eV. The insert shows a dependence of a ratio μ of the area under C2 (the second component) $S_{\text{C-N}}$ with $E_b = 285.3$ eV to the full area S_{C1s} on the C1s-spectrum on υ.

It follows from Figure 5, d that the HOPG G1s-spectrum has a maximum when the binding energy $E_\text{b} = 284.4$ eV. The spectral line corresponds to the bonds C−C of graphite atoms, i. e. to sp^2-hybridization (see, for example, the studies [52,53]). A peak asymmetry at half maximum was 1.6 : 1. According to the study [54], the asymmetry of the C1s-spectrum is caused by presence of surface defects. In addition to this basic component, the HOPG C1s-spectrum includes an additional component when $E_\text{b} = 290.8$ eV (the bond $\pi-\pi^*$, the shake-up satellite), which by the binding energy is removed by 6.4 eV from the base peak. It corresponds to a peak of losses of weakly bound π-electrons and characterizes the graphite material [55]. The third weakly-intensive peak with the binding energy of 286.7 eV can be due to the influence of trace amounts of oxygen that is adsorbed on the surface and interacts with carbon [56]. The obtained XPS spectra are analyzed to show that the peak intensities of the C1s-spectra of all the LIG samples synthesized at the various speeds also correspond to the binding energy of 284.4 eV.

However, the forms of the lines of the C1s-spectra of the LIGs synthesized at the various conditions noticeably differ from each other by full width at half maximum, ΔE_{C1s}. It is clear from Figure 8, a that shows a decrease of ΔE_{C1s} with an increase of υ. With increase of the scanning speed, ΔE_{C1s} approaches the value of 1.35 eV that is obtained for the HOPG C1s-spectrum. Thus, with decrease of υ, the C1s-spectrum is broadened. The C1s-spectrum of the sample υ_10_P_0.55 produced at the lowest speed $\upsilon = 10$ mm/s can be decomposed into five components (Figure 5, a), whose maximums correspond to the following values of E_b (to the chemical bonds): 284.4 eV (C−C, sp^2), 285.3 eV (C−N),

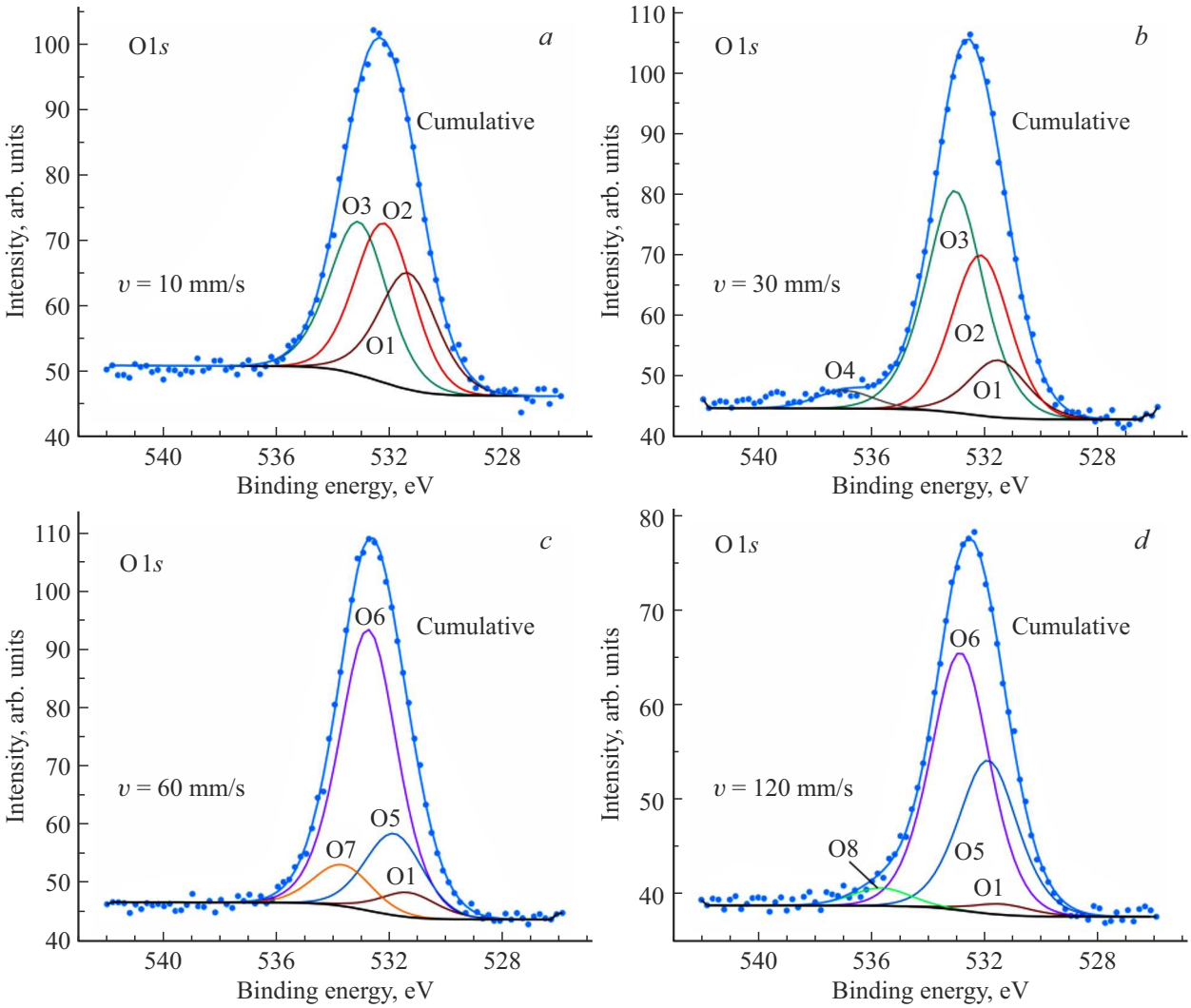

Figure 6. O1s-spectra of the LIG samples synthesized at $v = 10$ (a), 30 (b), 60 (c), 120 mm/s (d). The peaks O1, O2, O3, O4, O5, O6, O7 and O8 correspond to the binding energies 531.4, 532.2, 533.2, 537.0, 532.0, 532.8, 533.8 and 535.7 eV, respectively.

286.7 eV (C−O), 288.5 eV (C=O), 290.8 eV ($\pi-\pi^*$). The binding energies of the first ones of these peaks coincide with data obtained in the studies [32,57]. It is noteworthy that the ratio μ of the area $S_{\text{C-N}}$ under C2 (the second component) with $E_b = 285.3$ eV to the full area S_{C1s} of the C1s spectrum decreases rapidly with increase of v (Figure 5, a, the insert), so that this components is absent in the C1s-spectrum of the sample v_120_P_2.0 synthesized when $v = 120$ mm/s (Figure 5, c).

It follows from Figure 6 that the O1s-spectrum of the sample v_10_P_0.55 can be decomposed into three components (O1, O2 and O3) with the binding energies 531.4, 532.2 and 533.2 eV. According to the studies [58–60], the peaks O1, O2 and O3 can be assigned to bonds of quinine carbonyl oxygen, O=C and O−C, respectively. Decomposition of the O1s-spectrum of the sample v_30_P_0.8 has an additional peak O4 with the binding energy of 537.0 eV, which can be assigned to bonds C−H_2O [61]. The sample v_60_P_1.2 is characterized by the peak O1 and the three other peaks O5, O6 and O7 with the binding energies 532.0, 532.8 and 533.8 eV, respectively. According to the study [62], the peak O7 can be related to adsorbed moisture. The O1s-spectrum of the sample v_120_P_2.0 can be decomposed into four components — O1, O5, O6 and O8 with the maximum value of the last one at the binding energy of 535.7 eV. It is difficult to precisely identify all the above-listed peaks, since values of the binding energy of the same type of the chemical bond given by many authors from the known literature sources differ from each other by at least 0.1 eV. But Figure 6 clearly shows that the laser beam scanning speed in a complex way affects the O1s-spectrum during its synthesis.

It follows from Figure 7 that the N1s-spectrum of the sample v_10_P_0.55 can be decomposed into three nitrogen components, N1, N2 and N3, with peak values of the binding energy 399.0, 400.1 and 401.5 eV, which correspond to the pyridinic N, pyrrolic N and graphitic N [53,63–65] configurations, respectively. They belong to the nitrogen

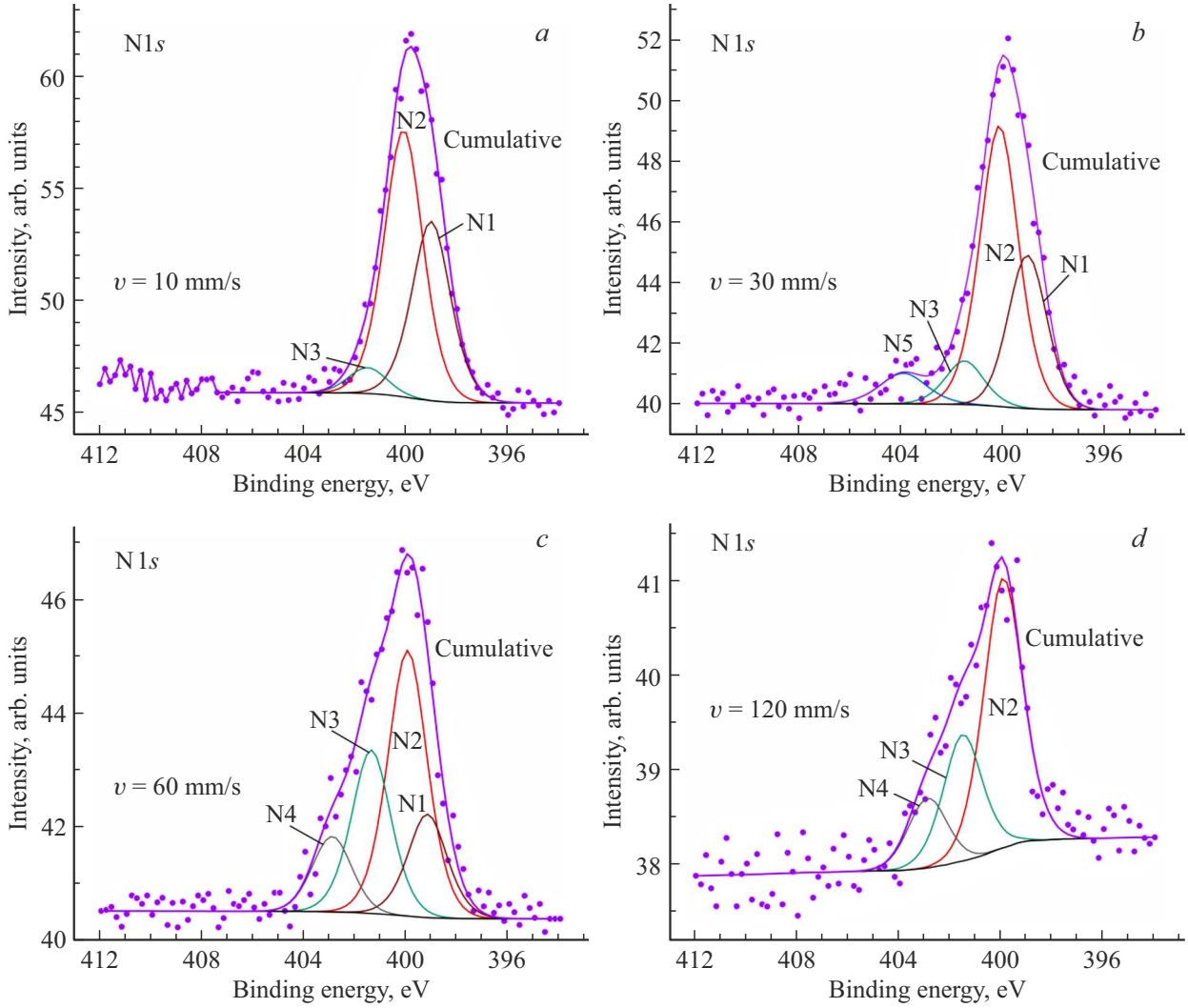

Figure 7. N1s-spectra of the LIG samples synthesized at $v = 10$ (a), 30 (b), 60 (c), 120 mm/s (d), with the decomposition peaks that correspond to a pyridinic N1 ($E_b = 399.0$ eV), a pyrrolic N2 ($E_b = 400.1$ eV), a graphitic N3 ($E_b = 401.5$ eV) configuration. The peaks N4 and N5 with $E_b = 402.9$ and 403.9 eV correspond to oxidized nitrogen of the pyridinic configuration and nitrite NO_2^-, respectively.

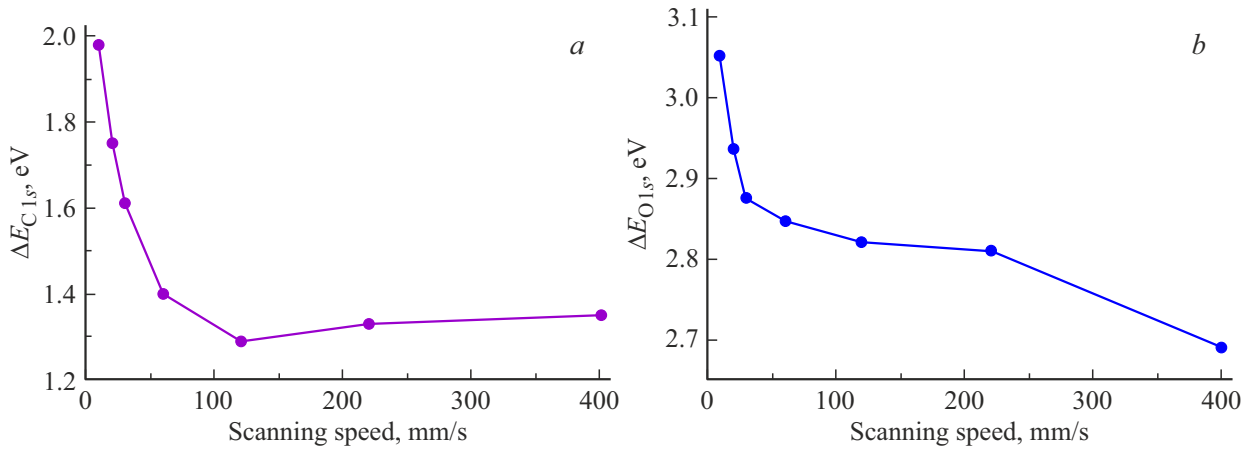

Figure 8. Dependences of full width at half maximum for the bands C1s (a) and O1s (b) of the XPS spectra of the LIG samples on the laser beam scanning speed during their synthesis.

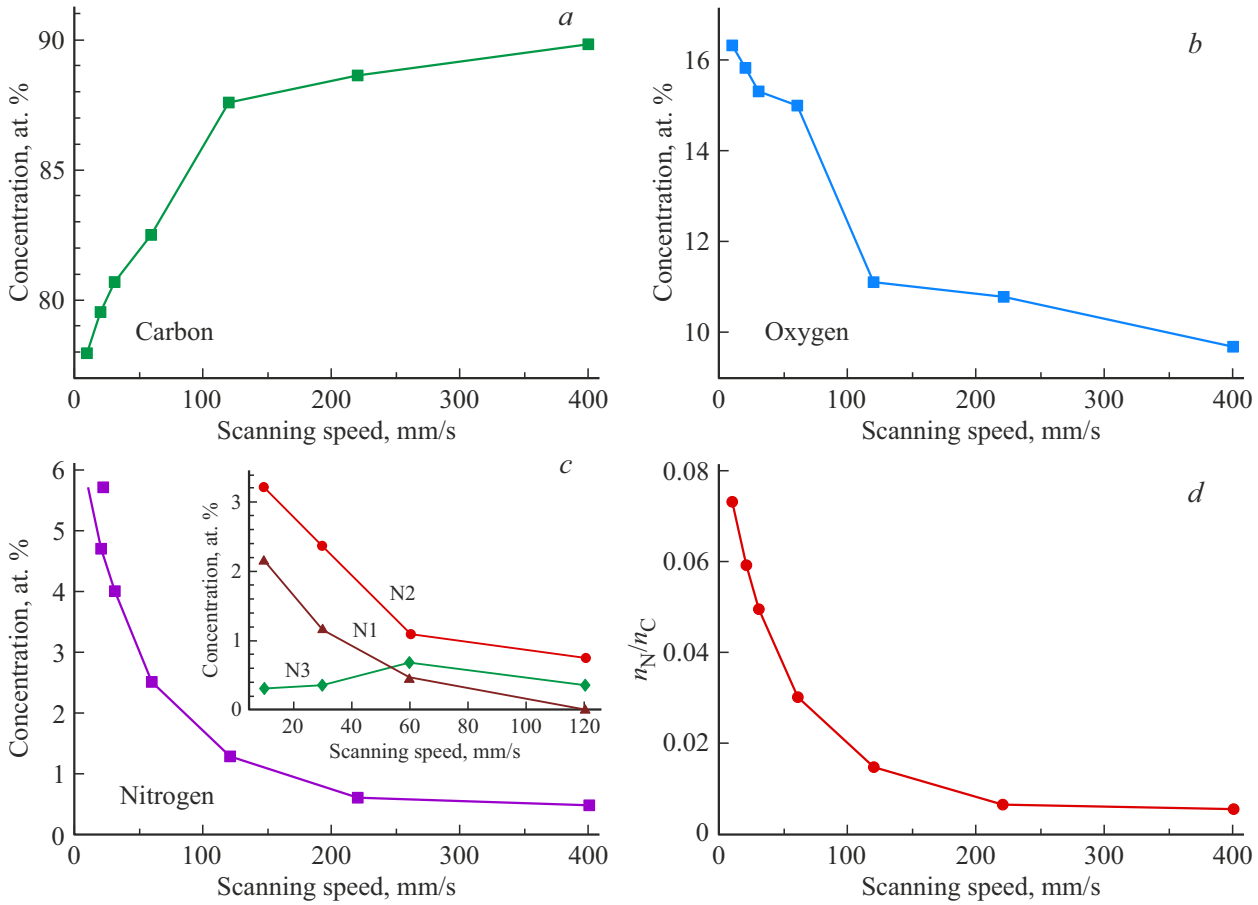

Figure 9. Dependences: of the concentration of atoms of carbon n_C (a), oxygen n_O (b) and nitrogen n_N (c); of the ratio n_N/n_C (d) in the subsurface layer of the LIG on the laser beam scanning speed. The insert shows the dependences of the concentrations of the pyridinic (N1), pyrrolic (N2) and graphitic (N3) nitrogen configurations on the scanning speed.

atoms that are in the various configurations of the crystal structure of defective graphene [63]. The N1s-spectra of the samples v_60_P_1.2 and v_120_P_2.0 have additional peaks with the nitrogen binding energy N4. It corresponds to 402.9 eV, which according to the study [66] can be ascribed to oxidized nitrogen of the pyridinic configuration (N^+-O^-), i. e. to the nitrogen atom bound to two carbon atoms and one oxygen atom. It is noteworthy that the binding energies of the four listed nitrogen configurations that are listed above coincide with the values obtained in the studies [66,67]. The N1s-spectrum of the sample v_30_P_0.8 is distinguished by that its decomposition has a peak with the binding energy of 403.9 eV, which corresponds to nitrite NO_2^- [68,69].

The C1s-, O1s- and N1s-spectra of the synthesized samples allowed determining the influence of the scanning speed on the concentrations n_C, n_O and n_N of carbon, oxygen and nitrogen, respectively, therein (Figure 9). It is clear that the increase of the concentration of oxygen and nitrogen with decrease of the scanning speed v is accompanied by the decrease of the carbon concentration. With the decrease of v within the entire range of its variation, the decrease and the increase of the concentrations of carbon and oxygen are by 1.15 and 1.68 times, respectively. At the same time, it follows from the obtained data that the nitrogen concentrations in the subsurface layer of the LIG synthesized at $v = 10$ mm/s, $P_{opt} = 0.55$ W and $v = 400$ mm/s, $P_{opt} = 4.5$ W are 5.7 and 0.5 at.%, respectively. It means that by decreasing the laser beam scanning speed from 400 to 10 mm/s and selecting the laser power it is possible to increase the nitrogen concentration in the synthesized carbon material in more than 11 times. At the same time, according to data from the insert of Figure 9, c, the concentrations n_{N1}, n_{N2} and n_{N3}, of the various nitrogen forms N1, N2 and N3, respectively, depend on $v$following the different patterns. It is clear that the total nitrogen concentration significantly increases with reduction of the speed v due to the increase of the concentrations of the pyridinic and pyrrolic nitrogen configurations. It is noteworthy that a specific concentration of all the nitrogen atoms in the nanocrystalline structure of carbon monotonically increases with the decrease of v (Figure 9, d). Thus, during LIG synthesis it is self-doped with nitrogen, wherein the lower the scanning speed, the higher the nitrogen concentration. Doping the carbon material with nitrogen shall result in decrease of its electric

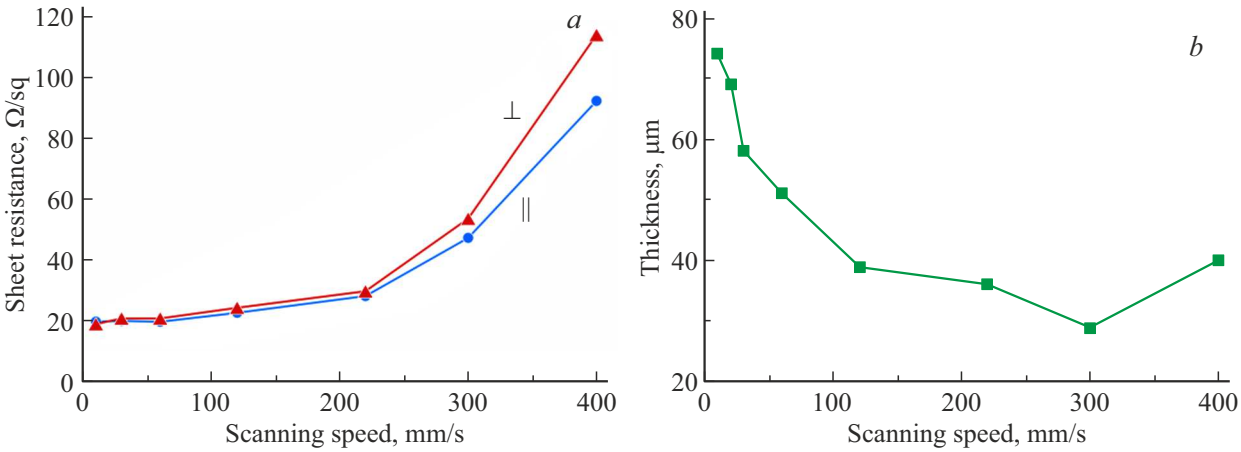

Figure 10. *a* — the sheet resistance of the LIG, which is measured by the four-probe method parallel (||) and perpendicular (⊥) to laser beam scanning lines; *b* — the LIG thickness as a function of the scanning speed.

resistance, which is exactly observed in the experiment (Figure 10, *a*). It is clear from the figure that indeed with the decrease of v from 400 to 10 mm/s the values of the sheet resistance of the samples synthesized at $P = P_{opt}$ decreaseby several times. It should be noted that self-doping of the synthesized material with nitrogen at the small v is just one of the causes of a decrease of the sheet resistance. With the decrease of v there is a noticeable increase of the thickness of the LIG film structure (Figure 10, *b*) and its density [2], which also contributes to the decrease of its sheet resistance.

The above-given results of the studies of the composition of the LIG film structure are attributed to its subsurface layer. Meanwhile, it is known that the LIG composition can be inhomogeneous with depth, which is indicated by the different Raman spectra recorded at the various section points of the LIG film structure, which are at the different depths [14]. Investigation of variation of the composition and the properties of the LIG depending on its depth is a separate nontrivial problem and can be an object of further research in the future.

4. Conclusion

We have studied the influence of the line-by-line scanning speed of the focused beam of the continuous-wave laser on the chemical composition of the nanocarbon film structure that is synthesized on the surface of the polyimide film during its laser pyrolysis. We obtained the XPS spectra for the LIG samples that are synthesized within the range of the scanning speeds v from 10 to 400 mm/s and at the powers that provide maximum electric capacitance. The synthesized LIG samples exhibited the peaks C1s, O1s and N1s that correspond to the atoms of carbon, oxygen and nitrogen, respectively. It is shown that with the increase of the speed v the width of the C1s-spectrum significantly decreases. The N1s-spectrum of the LIG sample produced at $v = 10$ mm/s is deconvoluted to show that the nitrogen atoms in the nanocrystalline structure of the graphite material are in the pyridinic, pyrrolic and graphitic configurations, wherein the concentrations of the first two configurations decrease with the increase of v. With the decrease of the scanning speed from 400 to 10 mm/s, the nitrogen concentration in the LIG's subsurface layer increases 11.4-fold to 5.7 at.%, whereas the carbon concentration decreases 1.15-fold from 89.8 to 78 at.%. The increase of the nitrogen concentration in the synthesized film material is accompanied by the decrease of its sheet resistance and is in agreement with a previously found pattern on a significant increase of electric capacitance of the LIG with a decrease of the line-by-line scanning speed during its synthesis to 10 mm/s.

Acknowledgments

The authors would like to thank K.G. Mikheev (The Udmurt Federal Research Center, Ural Branch of RAS) for the studies using the Raman-scattering spectrometer.

Funding

The study was carried out within the framework of the state assignment of the Ministry of Science and Higher Education of the Russian Federation (the registration number 1022040600237-3-1.3.2). The experiments have been carried out using the equipment provided by the Common Use Center of „Center of Physical and Physicochemical Methods of Analysis and Study of the Properties and Surface Characteristics of Nanostructures, Materials, and Products“ of the Udmurt Federal Research Center, Ural Branch of RAS.

Conflict of interest

The authors declare that they have no conflict of interest.

References

[1] J. Lin, Z. Peng, Y. Liu, F. Ruiz-Zepeda, R. Ye, E.L.G. Samuel, M.J. Yacaman, B.I. Yakobson, J.M. Tour. Nature Commun. **5**, 5714 (2014).

[2] R.G. Zonov, K.G. Mikheev, D.L. Bulatov, T.N. Mogileva, A.V. Syugaev, G.M. Mikheev. Diam. Relat. Mater. **157**, 112529 (2025).

[3] M. Dosi, I. Lau, Y. Zhuang, D.S.A. Simakov, M.W. Fowler, M.A. Pope. ACS Appl. Mater. Interfaces **11**, *6*, 6166 (2019).

[4] M.G. Stanford, K. Yang, Y. Chyan, C. Kittrell, J.M. Tour. ACS Nano **13**, *3*, 3474 (2019).

[5] C. Francis, A. Rektor, T. Valayil-Varghese, N. McKibben, I. Estrada, J. Forbey, D. Estrada. Front. Chem. **12**, 1448205 (2024).

[6] K.G. Mikheev, R.G. Zonov, D.L. Bulatov, A.E. Fateev, G.M. Mikheev. Tech. Phys. Lett. **46**, *5*, 458 (2020).

[7] Y.P. Suhorukov, A.V. Telegin, K.G. Mikheev, R.G. Zonov, L.I. Naumova, G.M. Mikheev. Opt. Mater. (Amst.) **133**, 112957 (2022).

[8] Y. Wang, C. Han, Y. Zhou, C. Ke, Y. Fan, Y. Yang, Z. Chen, Y.S. Wang. Carbon Trends **11**, 100255 (2023).

[9] J. Liu, H. Ji, X. Lv, C. Zeng, H. Li, F. Li, B. Qu, F. Cui, Q. Zhou. Microchimica Acta **189**, *2*, 54 (2022).

[10] T.S.D. Le, H.P. Phan, S. Kwon, S. Park, Y. Jung, J. Min, B.J. Chun, H. Yoon, S.H. Ko, S.W. Kim, Y.J. Kim. Adv. Funct. Mater. **32**, *48*, 2205158 (2022).

[11] W. Song, J. Zhu, B. Gan, S. Zhao, H. Wang, C. Li, J. Wang. Small **14**, *1*, 1702249 (2018).

[12] A.V. Syugaev, R.G. Zonov, K.G. Mikheev, A.N. Maratkanova, G.M. Mikheev. J. Phys. Chem. Solids **181**, 111533 (2023).

[13] A. Velasco, Y.K. Ryu, A. Hamada, A. de Andrés, F. Calle, J. Martinez. Nanomater. **13**, *5*, 788 (2023).

[14] K.G. Mikheev, A.V. Syugaev, R.G. Zonov, D.L. Bulatov, G.M. Mikheev. Phys. Solid State **65**, *2*, 347 (2023).

[15] S.G. Jo, R. Ramkumar, J.W. Lee. Chem. Sus. Chem. **17**, *5*, e202301146 (2024).

[16] H. Liu, Y. Xie, J. Li, Z. Sun, J. Liu, K. Moon, L. Lu, Y. Chen, Y. Tang, X. Chen, C.P. Wong. Chem. Eng. J. **404**, 126375 (2021).

[17] M. Wu, F. Wang, X. Gao, Y. Li, C. Zhang, Y. Bao, Y. Ruan, M. Zhang, Z. Su. Diam. Relat. Mater. **150**, 111701 (2024).

[18] H. Zhang, J. Li, M. Sheng, Y. Guo, S. Guo, Y. Li. Diam. Relat. Mater. **144**, 111055 (2024).

[19] Y. Houeix, S. Habboush, S. Gomez-Gijon, N. Rodriguez, F.J. Romero, A. Rivadeneyra. Flex. Print. Electron. **9**, *3*, 035010 (2024).

[20] J. Vandervelde, Y. Yoon, R. Shahriar, S.B. Cronin, Y. Chen. Small Sci. **5**, *6*, 2500022 (2025).

[21] Q. Zhang, F. Zhang, X. Liu, Z. Yue, X. Chen, Z. Wan. Adv. Mater. Technol. **8**, *16*, 2300244 (2023).

[22] J.D. Kim, T. Kim, J. Pak. Trans. Korean Inst. Electr. Eng. **67**, *3*, 406 (2018).

[23] K.G. Mikheev, R.G. Zonov, T.N. Mogileva, A.E. Fateev, G.M. Mikheev. Opt. Laser Technol. **141**, 107143 (2021).

[24] J. de la Roche, I. López-Cifuentes, A. Jaramillo-Botero. Carbon Lett. **33**, *2*, 587 (2023).

[25] K.G. Mikheev, R.G. Zonov, A.V. Syugaev, D.L. Bulatov, G.M. Mikheev. Phys. Solid State **64**, *5*, 579 (2022).

[26] M. Burke, C. Larrigy, E. Vaughan, G. Paterakis, L. Sygellou, A.J. Quinn, G. Herzog, C. Galiotis, D. Iacopino. ACS Omega **5**, *3*, 1540 (2020).

[27] V.M. Styapshin, I.A. Zlobin, K.G. Mikheev, E.I. Ryabov, G.M. Mikheev. Bulletin of the Lebedev Physics Institute **52**, *Suppl 4*, S429 (2025).

[28] V.S. Antropova, I.A. Zlobin, G.M. Mikheev. Journal of Applied Spectroscopy **92**, *4*, 727 (2025).

[29] A. Rabti, S. Baachaoui, M. Zouari, N. Raouafi. J. Pharm. Biomed. Anal. Open **5**, 100069 (2025).

[30] M. Liu, J.N. Wu, H.Y. Cheng. Sci. China Technol. Sci. **65**, *1*, 41 (2022).

[31] R.G. Zonov, K.G. Mikheev, A.A. Chulkina, I.A. Zlobin, G.M. Mikheev. Diam. Relat. Mater. **148**, 111409 (2024).

[32] M. Khandelwal, C.V. Tran, J.B. In. Appl. Surf. Sci. **576**, *Part A*, 151714 (2022).

[33] M. Khandelwal, C.V. Tran, J. Lee, J.B. In. Chem. Eng. J. **428**, 131119 (2022).

[34] T. Feurer, R. Sauerbrey, M.C. Smayling, B.J. Story. Appl. Phys. A **56**, *3*, 275 (1993).

[35] A. Basu, K. Roy, N. Sharma, S. Nandi, R. Vaidhyanathan, S. Rane, C. Rode, S. Ogale. ACS Appl. Mater. Interfaces **8**, 31841 (2016).

[36] J. Cai, C. Lv, C. Hu, J. Luo, S. Liu, J. Song, Y. Shi, C. Chen, Z. Zhang, S. Ogawa, E. Aoyagi, A. Watanabe. Energy Storage Mater. **25**, 404 (2020).

[37] Z. Wan, M. Umer, M. Lobino, D. Thiel, N.-T. Nguyen, A. Trinchi, M.J.A. Shiddiky, Y. Gao, Q. Li. Carbon **163**, 385 (2020).

[38] K.G. Mikheev, R.G. Zonov, D.L. Bulatov, A.V. Syugaev, G.M. Mikheev. Tech. Phys. Lett. **50**, *10*, 51 (2025).

[39] M. He, Y. Wang, S. Wang, S. Luo. Carbon **168**, 308 (2020).

[40] S. Bai, L. Ruan, H. Chen, Y. Du, H. Deng, N. Dai, Y. Tang. Chem. Eng. J. **493**, 152805 (2024).

[41] L.X. Duy, Z. Peng, Y. Li, J. Zhang, Y. Ji, J.M. Tour. Carbon **126**, 472 (2018).

[42] K.G. Mikheev, R.G. Zonov, N.V. Chuchkalov, G.M. Mikheev. Phys. Solid State **66**, *2*, 268 (2024).

[43] G. Bhattacharya, S.J. Fishlock, S. Hussain, S. Choudhury, A. Xiang, B. Kandola, A. Pritam, N. Soin, S.S. Roy, J.A. McLaughlin. ACS Appl. Mater. Interfaces **14**, *27*, 31109 (2022).

[44] A. Eckmann, A. Felten, I. Verzhbitskiy, R. Davey, C. Casiraghi. Phys. Rev. B **88**, *3*, 035426 (2013).

[45] A.C. Ferrari, D.M. Basko. Nature Nanotechnol. **8**, *4*, 235 (2013).

[46] D.W. Boukhvalov, I.S. Zhidkov, A. Kiryakov, J.L. Menéndez, L. Fernández-García, A.I. Kukharenko, S.O. Cholakh, A.F. Zatsepin, E.Z. Kurmaev. Nanoscale Res. Lett. **16**, *1*, 153 (2021).

[47] A.C. Ferrari, J.C. Meyer, V. Scardaci, C. Casiraghi, M. Lazzeri, F. Mauri, S. Piscanec, D. Jiang, K.S. Novoselov, S. Roth, A.K. Geim. Phys. Rev. Lett. **97**, *18*, 187401 (2006).

[48] D.L. Mafra, G. Samsonidze, L.M. Malard, D.C. Elias, J.C. Brant, F. Plentz, E.S. Alves, M.A. Pimenta. Phys. Rev. B **76**, *23*, 233407 (2007).

[49] N. Kumar, R. Pandian, P.K. Das, T.R. Ravindran, S. Dash, A.K. Tyagi. J. Phys. D: Appl. Phys. **46**, *39*, 395305 (2013).

[50] L.G. Cançado, K. Takai, T. Enoki, M. Endo, Y.A. Kim, H. Mizusaki, A. Jorio, L.N. Coelho, R. Magalhães-Paniago, M.A. Pimenta. Appl. Phys. Lett. **88**, *16*, 163106 (2006).

[51] A. Eckmann, A. Felten, A. Mishchenko, L. Britnell, R. Krupke, K.S. Novoselov, C. Casiraghi. Nano Lett. **12**, *8*, 3925 (2012).

[52] J.L. Hueso, J.P. Espinós, A. Caballero, J. Cotrino, A.R. González-Elipe. Carbon **45**, *1*, 89 (2007).
[53] A. Ghosh, S. Kaur, G. Verma, C. Dolle, R. Azmi, S. Heissler, Y.M. Eggeler, K. Mondal, D. Mager, A. Gupta, J.G. Korvink, D.-Y. Wang, A. Sharma, M. Islam. ACS Appl. Mater. Interfaces **16**, *31*, 40313 (2024).
[54] D.-Q. Yang, E. Sacher. Langmuir **22**, *3*, 860 (2006).
[55] A. Ashraf, S.A. Dastgheib, G. Mensing, M.A. Shannon. J. Supercrit. Fluids **76**, 32 (2013).
[56] X. Chen, X. Wang, D. Fang. Fullerenes Nanotubes. Carbon Nanostructures **28**, *12*, 1048 (2020).
[57] A.K. Thakur, B. Lin, F.H. Nowrin, M. Malmali. ACS Environ. Sci. Technol. Water **2**, *1*, 75 (2022).
[58] S. Alotibi, T.F. Qahtan, A.M. Alansi, T.O. Owolabi, S.T. Hameed, N. Afzal, S. Bilal, D. Salah. Coatings **14**, *5*, 534 (2024).
[59] J.-H. Zhou, Z.-J. Sui, J. Zhu, P. Li, D. Chen, Y.-C. Dai, W.-K. Yuan. Carbon **45**, *4*, 785 (2007).
[60] K.C. Yung, D.W. Zeng, T.M. Yue. Appl. Surf. Sci. **173**, *3–4*, 193 (2001).
[61] G. Simões dos Reis, C.M. Subramaniyam, A. Duarte Cárdenas, S.H. Larsson, M. Thyrel, U. Lassi, F. García-Alvarado. ACS Omega **7**, *46*, 42570 (2022).
[62] J. Onoe, K. Takeuchi, K. Ohno, Y. Kawazoe. J. Vac. Sci. Technol. A **16**, *2*, 385 (1998).
[63] C. Zhang, L. Fu, N. Liu, M. Liu, Y. Wang, Z. Liu. Adv. Mater. **23**, *8*, 1020 (2011).
[64] F.M. Hassan, V. Chabot, J. Li, B.K. Kim, L. Ricardez-Sandoval, A. Yu. J. Mater. Chem. A **1**, *8*, 2904 (2013).
[65] V.V. Bolotov, P.M. Korusenko, S.N. Nesov, S.N. Povoroznyuk, Yu.A. Sten'kin. Omskii nauchnyi vestnik **4** (148), 119 (2016). (in Russian).
[66] Y. Shao, S. Zhang, M.H. Engelhard, G. Li, G. Shao, Y. Wang, J. Liu, I.A. Aksay, Y. Lin. J. Mater. Chem. **20**, *35*, 7491 (2010).
[67] Y. Wang, Y. Shao, D.W. Matson, J. Li, Y. Lin. ACS Nano **4**, *4*, 1790 (2010).
[68] F. Munakata, Y. Akimune, Y. Shichi, M. Akutsu, H. Yamaguchi, Y. Inoue. Chem. Commun. **1**, 63 (1997).
[69] N. Tabet, M. Faiz, A. Al-Oteibi. J. Electron Spectrosc. Relat. Phenomena **163**, *1–3*, 15 (2008).

Translated by M.Shevelev